

## A compressive sensing-based approach for Preisach hysteresis model identification

This content has been downloaded from IOPscience. Please scroll down to see the full text.

2016 Smart Mater. Struct. 25 075008

(<http://iopscience.iop.org/0964-1726/25/7/075008>)

View [the table of contents for this issue](#), or go to the [journal homepage](#) for more

Download details:

IP Address: 35.8.11.3

This content was downloaded on 20/07/2016 at 15:42

Please note that [terms and conditions apply](#).

# A compressive sensing-based approach for Preisach hysteresis model identification\*

Jun Zhang<sup>1,3</sup>, David Torres<sup>2</sup>, Nelson Sepúlveda<sup>2</sup> and Xiaobo Tan<sup>2,4</sup>

<sup>1</sup>Department of Electrical and Computer Engineering, University of California, San Diego, La Jolla, CA 92093, USA

<sup>2</sup>Department of Electrical and Computer Engineering, Michigan State University, East Lansing, MI 48824, USA

E-mail: j5zhang@ucsd.edu, torresd5@egr.msu.edu, nelsons@egr.msu.edu and xbtan@egr.msu.edu

Received 23 December 2015, revised 18 March 2016

Accepted for publication 14 April 2016

Published 24 May 2016



## Abstract

The Preisach hysteresis model has been adopted extensively in magnetic and smart material-based systems. Fidelity of the model hinges on accurate identification of the Preisach density function. Existing work on the identification of the density function usually involves applying an input that provides sufficient excitation and measuring a large set of output data. In this paper, we propose a novel compressive sensing-based approach for Preisach model identification that requires fewer measurements. The proposed approach adopts the discrete cosine transform of the output data to obtain a sparse vector, where the order of all the output data is assumed to be known. The model parameters can be efficiently reconstructed using the proposed scheme. For comparison purposes, a constrained least-squares scheme using the same number of measurements is also considered. The root-mean-square error is adopted to examine the model identification performance. The proposed identification approach is shown to have better performance than the least-squares scheme through both simulation and experiments involving a vanadium dioxide (VO<sub>2</sub>)-integrated microactuator.

Keywords: hysteresis, Preisach model, compressive sensing, identification, vanadium dioxide, DCT transform

(Some figures may appear in colour only in the online journal)

## 1. Introduction

Hysteresis is a phenomenon found in ferromagnetic materials [1–5] and various classes of smart materials [6–16]. Unlike physics-based hysteresis models that are often derived based on specific physical properties [1], phenomenological hysteresis models are often constructed based on input and output data, and are more extensively utilized in practical applications. Examples of reported phenomenological hysteresis models are Preisach model [2–6, 17], Prandtl–Ishlinskii model [7, 8], Maxwell model [9, 10], Bouc–Wen model [11, 12], and Duhem model [13, 14]. Preisach model is one of

the most popular and effective hysteresis models and it has proven effective in characterizing various systems with hysteresis.

A Preisach model consists of weighted superposition of hysterons. Practical parameter identification involves discretization of the Preisach density function in one way or another, and one effective method is to approximate the density function with a piecewise constant function [5]. Both online [2, 17] and offline [3–6] schemes can be adopted for model identification. When the discretization level is  $L$ , there are  $L(L + 1)/2$  cells with different density values [18]. The input needs to provide sufficient excitation for all the density values for model identification [2]. One example of such inputs takes the form of damped oscillations, which produces nested hysteresis loops [2]. The input sequence should contain at least  $L(L + 1)/2$  elements to identify all the densities. When the discretization level is chosen larger, the

\* This work was supported by the National Science Foundation (CMMI 1301243).

<sup>3</sup> This work was done when Jun Zhang was a graduate student at Michigan State University.

<sup>4</sup> Author to whom any correspondence should be addressed.

corresponding Preisach model could better capture the actual hysteresis, but the identification would require a larger number of measurements. For instance, in [4], the Preisach density function was discretized into 200 levels, and at least 20 100 measurements would need to be taken and processed to identify all the density values. In [6], a 20-level Preisach model was adopted to characterize the displacement-temperature hysteresis of a vanadium dioxide (VO<sub>2</sub>)-coated micro-actuator. In order to capture the hysteresis under quasi-static conditions, a relatively long wait time was needed for each measurement due to the slow thermal dynamics, resulting in long experiment time for collecting the required data for model identification [6]. Optimal compressions of the Preisach model and the generalized Prandtl–Ishlinskii model have been explored recently [19, 20]. While the compression schemes result in hysteresis models with fewer parameters, one still needs to identify high-fidelity hysteresis models before carrying out the compression procedures. Therefore, it is of great interest to design a more efficient identification approach for the Preisach model that requires fewer input–output data.

Compressive sensing is an alternative to Nyquist–Shannon sampling theory for acquisition and reconstruction of sparse signals. The compressive sensing theory [21–24] states that any length- $N$  signal  $q$  that can be well approximated using  $K$  coefficients can be faithfully recovered from  $M = O(K \log(N/K))$  random linear projections of the signal. Practically, many natural and man-made signals are sparse or compressible in the sense that they have compact representations in a transformed domain, through discrete Fourier transform (DFT) [25], discrete cosine transform (DCT) [26], or discrete Wavelet transform [27], etc. For example, in [26], audio signals were transformed using one-dimensional DCT, and the sparse DCT coefficients were reconstructed using a compressive sensing-based algorithm. The compressive sensing technique has been successfully applied in signal processing [27–29], networks [30, 31], machine learning [32], as well as system and control [25, 33]. However, there has been little work, if any at all, reported on the use of compressive sensing in hysteresis model identification.

In this paper we consider identifying the Preisach model using a novel compressive sensing-based approach that requires fewer measurements. The proposed approach adopts the DCT of the output data to obtain a sparse vector, where the order of all the output data is assumed to be known. The model parameters can be efficiently reconstructed using the proposed scheme. For comparison purposes, a constrained least-squares scheme using the same number of measurements is also considered. The root-mean-square error (RMSE) is adopted to examine the model identification performance. The proposed approach is first tested in simulation. For example, with 300 measurements, the RMSE error of model estimation based on the proposed approach is 79.2% smaller than that using the least-squares scheme. The advantage of the proposed approach is further verified in identifying the parameters of hysteresis between the voltage and the deflection of a VO<sub>2</sub>-integrated microactuator. On average, the RMSE error of the model estimation using the proposed approach is 17.8% smaller than that using the least-squares scheme.

A preliminary version of this work was presented at the 2015 American Control Conference [34]. The enhancements of this paper over [34] include (1) proposed compressive sensing-based approach that could generate sparser DCT coefficients and better model identification and estimation performances, (2) proofs to show that the matrix  $S$  associated with the Preisach plane memory curve is invertible under a given input sequence and the reconstruction error under noisy measurement is bounded, (3) extensive simulation and experimental studies on evaluating the performance of the proposed approach, and (4) improved structuring and presentation throughout the paper.

The remainder of the paper is organized as follows. In section 2, the Preisach model is briefly reviewed. The compressive sensing-based identification approach is presented in section 3. In section 4, detailed simulation results for the identification approach are presented. The effectiveness of the proposed approach is experimentally verified in section 5. Finally, concluding remarks and brief discussions on future work are presented in section 6.

## 2. Review of the Preisach model

In this section a brief overview of the Preisach model is provided. Readers are referred to [2, 3, 15, 16] for more details.

### 2.1. Preisach model

A Preisach model consists of weighted superposition of a continuum of *hystérons*. A generic hysteron,  $\gamma_{\beta,\alpha}$ , is a delayed relay characterized by a pair of thresholds  $(\beta, \alpha)$ . An initial condition  $u_{\beta,\alpha}(0) = \zeta_0(\beta, \alpha) \in \{-1, 1\}$  is needed to fully describe the behavior of the hysteron:

$$\gamma_{\beta,\alpha}[v(\cdot); \zeta_0(\beta, \alpha)] = \begin{cases} +1 & \text{if } v > \alpha, \\ -1 & \text{if } v < \beta, \\ \zeta_0(\beta, \alpha) & \text{if } \beta \leq v \leq \alpha, \end{cases} \quad (1)$$

where  $v(\cdot)$  denotes the input history  $v(\tau)$ ,  $0 \leq \tau \leq t$ .

The output of a Preisach operator  $\Gamma$ , with input  $v$  and initial condition  $\zeta_0 = \{\zeta_0(\beta, \alpha), \beta \leq \alpha\}$  can be represented as

$$u(t) = \Gamma[v(\cdot); \zeta_0](t) = \int_{\mathcal{P}_0} \mu(\beta, \alpha) \gamma_{\beta,\alpha}[v(\cdot); \zeta_0(\beta, \alpha)](t) d\beta d\alpha, \quad (2)$$

where  $\mu \geq 0$  is the density function. The *Preisach plane* is defined as  $\mathcal{P} = \{(\beta, \alpha) : \beta \leq \alpha\}$ . It often suffices to consider  $\mu$  with finite support  $\{(\beta, \alpha) : v_{\min} \leq \beta \leq \alpha \leq v_{\max}\}$  in  $\mathcal{P}$  due to input range constraints or physical saturation [3].

### 2.2. Discretization

For Preisach model identification, discretizing the density function  $\mu$  is typically conducted to obtain a finite number of parameters. A popular scheme is to approximate the density by a piecewise constant function—the density value  $\mu_{ij}$  is constant within cell  $(i, j)$ ,  $i = 1, 2, \dots, L$ ;  $j = 1, 2, \dots, L - i + 1$  [2]. Under this scheme, the Preisach model has  $L(L + 1)/2$

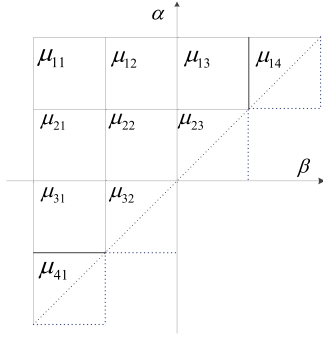


**Figure 1.** Illustration of a discretization of the Preisach density function, where the discretization level  $L = 4$ .

parameters, where  $L$  is the level of uniform discretization along  $\alpha$  (or equivalently,  $\beta$ ) direction in the Preisach plane. An example of Preisach model density function discretization is shown in figure 1. Note that the cells on the diagonal are assumed to have the same area as other cells in this work.

The output of the Preisach model (in the discrete-time setting) at time  $n$  is written as

$$\tilde{u}(n) = \mu_0 + \sum_{i=1}^L \sum_{j=1}^{L+1-i} \mu_{ij} s_{ij}(n), \quad (3)$$

where  $\mu_0$  is a bias constant,  $\mu_{ij}$  is the density value for cell  $(i, j)$ , and  $s_{ij}(n)$  denotes the *signed* area of the cell  $(i, j)$ , representing the collective effect from all the hysterons within cell  $(i, j)$ .

### 2.3. Identification procedure

To simplify the discussion, write all the model parameters into a column vector  $w = (w_1 \ w_2 \ \cdots \ w_{L(L+1)/2} \ \mu_0)^T$ , where  $w_k = \mu_{ij}$ ,  $k = (i-1)(2L-i+2)/2 + j-1$ . Apply an input sequence  $v[n]$ ,  $n = 1, 2, \dots, N$ , with sufficient excitation and then determine the corresponding  $s_{ij}[n]$  by tracking the evolution of the memory curve on the Preisach plane. Stack  $s_{ij}[n]$  into a row of a matrix:  $S(n, k) = s_{ij}(n)$ , and  $S(n, L(L+1)/2 + 1) = 1$ . The output vector of the model  $\tilde{u} = (\tilde{u}(1) \ \tilde{u}(2) \ \cdots \ \tilde{u}(N))^T$  can be expressed as

$$\tilde{u} = Sw. \quad (4)$$

Assume that the measured output under  $v[n]$  is expressed as  $b = (b(1) \ b(2) \ \cdots \ b(N))^T$ . The vector  $w$  can be determined such that  $\|Sw - b\|_2$  is minimized with the non-negative constraint imposed on all density values [3]. This constrained least-squares approach is denoted as ‘Least Squares’ in the figures for the remainder of the paper.

## 3. Compressive sensing-based Preisach model identification

### 3.1. Overview of compressive sensing

The compressive sensing theory [21–24] states that, if a length- $N$  signal  $p$  is  $K$ -sparse (namely,  $p$  contains no more

than  $K$  non-zero entries), then it is possible to faithfully recover  $p$  from its  $M = O(K \log(N/K)) \ll N$  random linear projections. In other words, consider

$$y = A\Phi p, \quad (5)$$

where  $y$  is an  $M \times 1$  vector of observations,  $A$  is an  $M \times N$  measurement matrix,  $\Phi$  is an  $N \times N$  basis transform matrix, and  $p$  is an  $N \times 1$   $K$ -sparse signal to be recovered. It is proven that the sparse signal  $p$  can be recovered if the matrix  $A\Phi$  satisfies the following restricted isometry property (RIP) condition [23]:

$$(1 - \delta_S) \|p\|_2^2 \leq \|A\Phi p\|_2^2 \leq (1 + \delta_S) \|p\|_2^2, \quad (6)$$

for all  $S$ -sparse signal  $p$ , where  $\delta_S > 0$  is the smallest isometry constant of matrix  $A\Phi$ . Based on [21],  $p$  can be recovered efficiently by solving the following  $l_1$  minimization problem:

$$\arg \min \|p\|_1 \text{ subject to } y = A\Phi p. \quad (7)$$

When  $A\Phi$  is a randomly sampled Gaussian matrix, Bernoulli matrix, or Fourier matrix, it satisfies the RIP condition with very high probability [22]. Practically, many natural and man-made signals are sparse or compressible in the sense that they have compact representations under DFT [25] or DCT [26].

The most common DCT definition [26] for one-dimensional signals  $x_1, x_2, \dots, x_N$  can be expressed as

$$X_d = \sum_{l=1}^N x_l \cos \frac{\pi}{N} \left( l + \frac{1}{2} \right) d, \quad (8)$$

where  $d = 1, 2, \dots, N$ . The resulting  $N \times N$  DCT matrix  $\Psi$  is orthogonal, whose elements can be written as

$$\Psi_{dl} = \cos \frac{\pi}{N} \left( l + \frac{1}{2} \right) d. \quad (9)$$

### 3.2. Compressive sensing for Preisach model

When the input sequence is chosen in the form of damped oscillations (an example of Preisach model with  $L = 30$  is shown in figure 2), the input sequence is known to produce sufficient excitation for all the density values [2]. The input levels are right at the cell walls, namely, each cell will be either 1 or  $-1$  in terms of the signed area. This particular input sequence is denoted as the ‘damped oscillation’ input sequence. The number of input values equals to the number of model parameters ( $N = L(L+1)/2 + 1$ ). It can be proved that the corresponding  $S$  is a full-rank  $N \times N$  matrix. Note that this paper only considers the ‘damped oscillation’ sequence, and other input sequences also exist such that the corresponding  $S$  is a full-rank  $N \times N$  matrix.

**Proposition 1.** Consider a Preisach model (written in the form of equation (4)) with discretization level  $L$ , and apply the ‘damped oscillation’ input sequence with  $N = L(L+1)/2 + 1$  elements. By tracking the evolution of the memory curve on the Preisach plane, the corresponding  $S$  is a full-rank  $N \times N$  matrix.

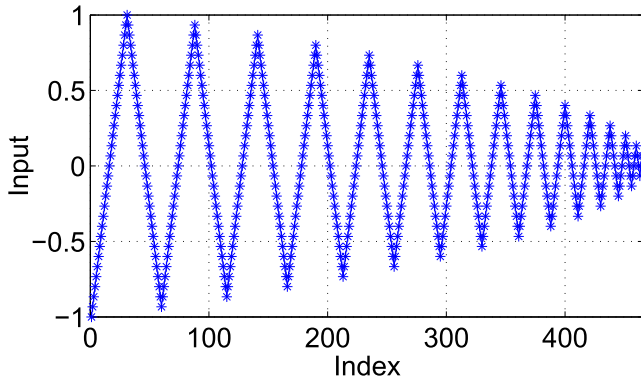


**Figure 2.** The ‘damped oscillation’ sequence for Preisach model identification ( $L = 30$ ).

**Proof.** Denote  $S_L$  the matrix  $S$  of the Preisach model with discretization level  $L$  under the damped oscillation input sequence. The proposition can be proved by mathematical induction as follows

(1) When  $L = 1$

$$\begin{aligned} \text{rank}(S_1) &= \text{rank} \begin{bmatrix} 0 & 1 \\ 1 & 1 \end{bmatrix}_{2 \times 2} \\ &= 2; \end{aligned} \quad (10)$$

(2) Assume that under the ‘damped oscillation’ input sequence with  $N = L(L + 1)/2 + 1$  elements,  $\text{rank}(S_L) = N$

(3) Under the damped oscillation input sequence with  $Z = (L + 1)(L + 1 + 1)/2 + 1 = N + L + 1$  elements, by reordering the rows and columns of corresponding  $S_{L+1}$

$$\begin{aligned} &\text{rank}(S_{L+1}) \\ &= \text{rank} \left( \begin{bmatrix} s_{1,1} & \cdots & s_{1,N+L+1} \\ \vdots & \ddots & \vdots \\ s_{N+L+1,1} & \cdots & s_{N+L+1,N+L+1} \end{bmatrix} \right)_{Z \times Z} \\ &= \text{rank} \left( \begin{bmatrix} s_{1,1} & \cdots & s_{1,N+L+1} \\ \vdots & \ddots & \vdots \\ s_{L+1,1} & \cdots & s_{L+1,N+L+1} \\ s_{2L+1,1} & \cdots & s_{2L+1,N+L+1} \\ s_{L+2,1} & \cdots & s_{L+2,N+L+1} \\ s_{2L+2,1} & \cdots & s_{2L+2,N+L+1} \\ \vdots & \ddots & \vdots \\ s_{N+L+1,1} & \cdots & s_{N+L+1,N+L+1} \end{bmatrix} \right)_{Z \times Z} \\ &= \text{rank} \left( \begin{bmatrix} 0 & \cdots & 1 & \vdots \\ \vdots & \ddots & \vdots & \vdots \\ 1 & \cdots & 1 & \vdots \\ \cdots & \cdots & \cdots & (S_L)_{N \times N} \end{bmatrix} \right)_{Z \times Z} \\ &= Z. \end{aligned} \quad (11)$$

The third equation is obtained by rearranging certain columns of the previous matrix, more specifically, by rearranging columns with column index  $1, L + 2, \dots, 1 + \frac{(l-1)(2L-l+4)}{2}, \dots, 1 + \frac{L(L+3)}{2}$ , where  $l = 1, 2, \dots, L + 1$ , to the left of the matrix.

So under ‘damped oscillation’ input sequence,  $S$  is a full-rank matrix.  $\square$

When only  $M < N$  output measurements,  $y_b$ , are available,  $y_b = (b(n_1) \ b(n_2) \ \cdots \ b(n_M))^T = Ab$ ,  $1 \leq n_1, n_2, \dots, n_M \leq N$ , where  $A$  is an  $M \times N$  matrix whose  $M$  rows are randomly chosen from  $N$  rows of an  $N \times N$  identity matrix, then

$$y_b = A \cdot Sw. \quad (12)$$

The number of measurements is less than the number of model parameters. A novel compressive sensing-based approach for identifying the Preisach model based on partial output measurements  $y_b$  is proposed.

In compressive sensing, a random measurement matrix is usually adopted to faithfully recover the sparse signals. Unfortunately, compressive sensing cannot be applied in the Preisach model identification directly. First, the matrix  $S$  in Preisach model identification must follow certain patterns (and thus cannot be chosen randomly) due to the Preisach plane structure. Second, since the input sequence for identification must provide sufficient excitation, the flexibility of designing the matrix  $S$  is further limited. Finally, the density vector  $w$  of the Preisach model is not necessarily sparse in its original domain.

Exploiting the fact that many natural and man-made signals are sparse in a transformed frequency domain, write

$$q = \Psi \cdot Sw \approx \Psi \cdot b, \quad (13)$$

where  $\Psi$  is an  $N \times N$  DCT matrix.  $q$  is thus an  $N \times 1$  column vector contains the DCT coefficients of  $Sw$ . It is found that  $q$  is approximately sparse in this work when the density values are spatially uniform, of a Gaussian profile, or generated randomly with each density value sampled from a uniform probability distribution, which is likely because of the damped oscillation structure of  $Sw$ . Since  $S$  is a full-rank matrix, the density values  $w$  can be expressed as

$$w = S^{-1}\Psi^{-1}q \quad (14)$$

and equation (12) can be rewritten as

$$y_b = ASS^{-1}\Psi^{-1}q = A\Psi^{-1}q. \quad (15)$$

When  $\Psi$  is chosen as the DCT matrix, the sparse signal  $q$  can be reconstructed via compressive sensing algorithm. The algorithm  $l_1$ -MAGIC is adopted to efficiently reconstruct the sparse signal  $q$  using a generic path-following primal-dual method [21]. The density parameter  $w$  can be obtained through equation (14) afterwards. This approach is denoted as ‘CS’.

The above compressive sensing-based approach only utilizes  $M$  input–output data to reconstruct the density values  $w$ . If the order of  $N$  output data is also known, denote  $b_{\text{order}} = (b(l_1) \ b(l_2) \ \cdots \ b(l_N))^T$ , such that  $b(l_1) \leq b(l_2) \leq \cdots \leq b(l_N)$ , then  $b_{\text{order}} = S_{\text{order}}w$ , and

$$q_{\text{order}} = \Psi \cdot S_{\text{order}}w \approx \Psi \cdot b_{\text{order}}. \quad (16)$$

The reconstruction scheme in [21] can still be adopted to identify the density  $w$ .  $q_{\text{order}}$  is found to be more approximately sparse than  $q$ , partially because  $S_{\text{order}}w$  is



monotonically increasing, and has more concentrated frequency components at low frequencies than that of  $S_w$ . It is verified in simulation and experiments that this approach generates better model reconstruction and model estimation performance. This approach is denoted as ‘CS Order’.

In order to facilitate the inverse compensation [5, 6] for dynamic hysteretic systems based on Preisach model, the density needs to be non-negative. The density  $w$ , as obtained in equation (14), is not necessarily non-negative. Based on the aforementioned ‘CS Order’ approach, a constrained least-squares approach can be further adopted as follows (denoted as ‘CS Order Non-negative’):

$$\min_w \|\Psi S_{\text{order}} \cdot w - q_{\text{order}}\|_2^2, \text{ where } w \geq 0. \quad (17)$$

When signal  $q$  is  $K$ -sparse and the measurements are without any noise, the density may be reconstructed with high accuracy. However, in simulation and experiments,  $q$  is found to be approximately sparse. In practical applications, the measurements are with measurement errors and noise. It is thus of practical importance to study the reconstruction performance for approximately sparse signals with measurement noise.

**Proposition 2.** Consider identifying the density  $w$  of a Preisach model using a compressive sensing algorithm [21], based on the expression of equation (14). With measurement noise, the actual measured data is  $y_b = A\Psi^{-1}q + e$ , where  $e$  is the measurement noise and  $\|e\|_2 \leq \epsilon$ . In our work,  $q_s$  is the truncated signal corresponding to the  $s$  largest absolute values of  $q$ , so the remaining  $N - s$  entries of  $q_s$  are zero. The numbers of entries of  $q_s$  and  $q$  are both  $N$ . The reconstruction of density  $w^*$  obeys

$$\|w^* - w\| \leq C_{1,s} \cdot \epsilon + C_{2,s} \cdot \frac{\|q - q_s\|_1}{\sqrt{s}}, \quad (18)$$

where  $C_{1,s}$ , and  $C_{2,s}$  are positive constants, and their values depend on  $s$ .

**Proof.**

$$\begin{aligned} \|w^* - w\|_2 &= \|S^{-1}\Psi^{-1}q^* - S^{-1}\Psi^{-1}q\|_2 \\ &\leq \|S^{-1}\Psi^{-1}\|_2 \cdot \|q^* - q\|_2 \\ &\leq \|S^{-1}\Psi^{-1}\|_2 \cdot \left( C'_{1,s} \cdot \epsilon + C'_{2,s} \cdot \frac{\|q - q_s\|_1}{\sqrt{s}} \right) \\ &\leq C_{1,s} \cdot \epsilon + C_{2,s} \cdot \frac{\|q - q_s\|_1}{\sqrt{s}}, \end{aligned} \quad (19)$$

where the second inequality can be proved based on [24]. When a specific input sequence is chosen, the 2-norm of  $S^{-1}\Psi^{-1}$  can also be calculated. The derivation can be similarly conducted for the other cases where the order of the output data are known.  $\square$

Note that the general formulation of compressive sensing algorithm requires that the transformation matrix  $\Psi$  has a dimension of  $N \times N$ . In order to utilize the compressive sensing framework to identify the Preisach model using equation (15), the dimension of the matrix  $S$  needs to be  $N \times N$ , which further requires that the initial input sequence

has  $N$  entries. For input sequence with a different number of entries, or that with  $N$  entries but the corresponding matrix  $S$  is not invertible, equation (15) cannot be adopted directly. Moore–Penrose pseudoinverse [35] could potentially be utilized as an approximation of the inverse of  $S$ . This paper considers cases where the input sequence has  $N$  entries and the corresponding  $S$  is invertible.

## 4. Simulation results

In this section, the proposed algorithms are tested in simulation for Preisach models with three different density profiles, namely, uniform profile, Gaussian profile, and random profile.

Consider a Preisach model with discretization level  $L = 30$ . The Preisach model has no bias ( $\mu_0 = 0$ ). Apply the ‘damped oscillation’ input sequence and obtain the corresponding output. The measured output is simulated with added noise that follows a uniform distribution on the interval  $[-5, 5]$ . In order to quantitatively examine the relationship between the reconstruction performance and the number of measurements, the compressive sensing-based identification approach is compared with a constrained least-squares scheme. The constrained least-squares method is realized with the Matlab command `lsqnonneg` to identify the vector of parameters that meets the sign constraints [3]. For each number of measurements used in the identification, simulation is run 1000 times (thus with different sets of density values and different sets of chosen input–output data), and the performance is averaged among all of the results.

### 4.1. Uniform profile

Consider a Preisach model which has the following uniform density profile

$$\mu_{ij} = 5, \quad (20)$$

where  $i = 1, 2, \dots; j = 1, 2, \dots, L - i + 1$ . Table 1 shows the normalized modeling error (RMSE and Maximum error) comparison between ‘Least Squares’, ‘CS’, ‘CS Order’, and ‘CS Order Non-negative’, when the number of measurements used for identification is 300. The error is obtained as follows: first, calculate the RMSE between the output of the identified Preisach model and that of the actual output, then divide the RMSE by the output range. Normalization of the RMSE facilitates the assessment of the algorithm performance. It is shown that ‘CS Order Non-negative’ produces the smallest modeling error, followed by ‘CS Order’, ‘CS’, and ‘Least Squares’.

### 4.2. Gaussian profile

Preisach densities with a Gaussian profile have been considered in the literature [2, 6]. Consider a Preisach model

**Table 1.** Comparison on the identification performance of Preisach model with a uniform density profile.

Scheme	RMSE	Max
Least Squares	0.0057	0.0411
CS	0.0039	0.0237
CS Order	0.0031	0.0221
CS Order Non-negative	0.0028	0.0175

**Table 2.** Comparison on the identification performance of Preisach model with a Gaussian density profile.

Scheme	RMSE	Max
Least Squares	0.0111	0.0620
CS	0.0049	0.0373
CS Order	0.0027	0.0137
CS Order Non-negative	0.0023	0.0124

which has the following Gaussian density profile

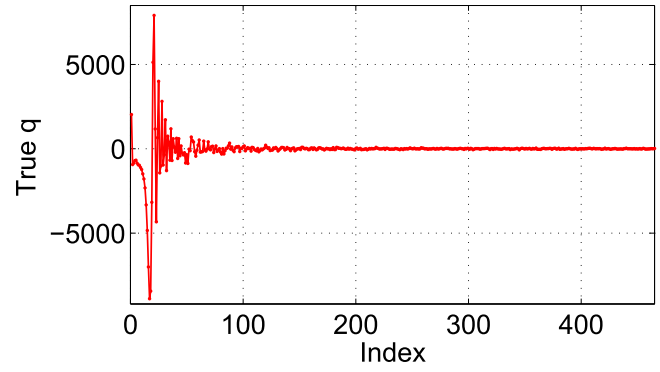
$$\mu_{ij} = 15 \exp\left(-\frac{(i - 15.5)^2 + (j - 15.5)^2}{60}\right), \quad (21)$$

where  $i = 1, 2, \dots; j = 1, 2, \dots, L - i + 1$ . Table 2 shows the normalized modeling error (RMSE and Maximum error) comparison between ‘Least Squares’, ‘CS’, ‘CS Order’, and ‘CS Order Non-negative’, when the number of measurements used for identification is 300. Similarly, it is shown that ‘CS’-based identification approaches produce better modeling performances.

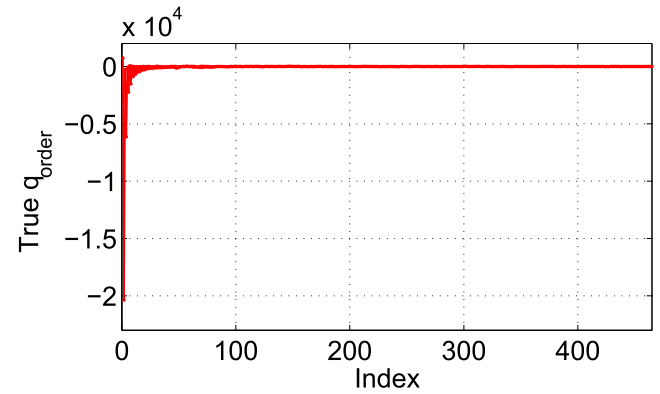
#### 4.3. Random profile

Consider a Preisach model which has the following random density profile: each of the 465 density values independently follows a uniform distribution on the interval  $[0, 12]$ . Figure 3(a) shows a typical example of  $q$ . It is seen that the dominant elements only concentrate at low frequency regions. The largest absolute value of elements in  $q$  is 8665.8, and as many as 363 elements are less than 1% of the largest elements of  $q$ . Figure 3(b) shows a typical example of  $q_{\text{order}}$ . It is seen that the dominant elements also cover the low frequencies. The largest absolute value of elements in  $q$  is 18 703.4, and it is found that 415 elements are less than 1% of the largest elements of  $q$ . It is verified in simulation that  $q_{\text{order}}$  is consistently more approximately sparse than  $q$ . It is thus expected that ‘CS Order’ would achieve better model reconstruction performance than ‘CS’. Figure 3(c) shows the reconstruction performance comparison of  $q$  between ‘CS’ and ‘CS Order’. It is evident that the ‘CS Order’ would achieve much better reconstruction performance. On average, the RMSE error of  $q_{\text{order}}$  based on ‘CS Order’ is 82.7% less than that of  $q$  using ‘CS’. It is noted that all  $N$  measurements are needed before ordering, and the advantage of the ‘CS Order’ approach is that fewer data is needed in reconstruction, and thus potentially more computation-efficient.

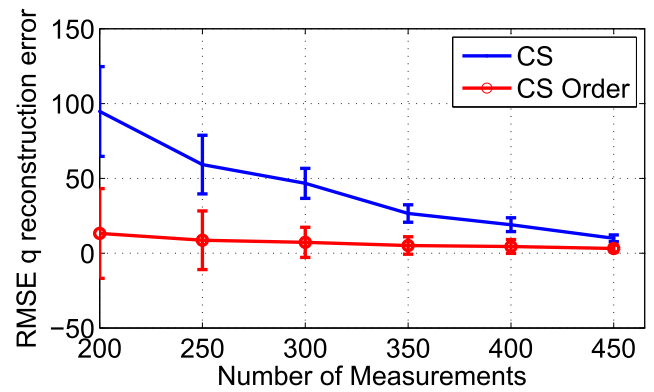
Figure 4(a) shows the reconstruction performance comparison of density  $w$  between ‘Least Squares’, ‘CS Without DCT’, ‘CS’, ‘CS Order’, and ‘CS Order Non-negative’, where ‘CS Without DCT’ directly uses the compressive sensing algorithm to identify the density  $w$  based on equation (12). It is shown that except the ‘CS Without DCT’, all of the CS-related reconstruction approaches result in better density reconstruction performances than that of the ‘Least



(a)

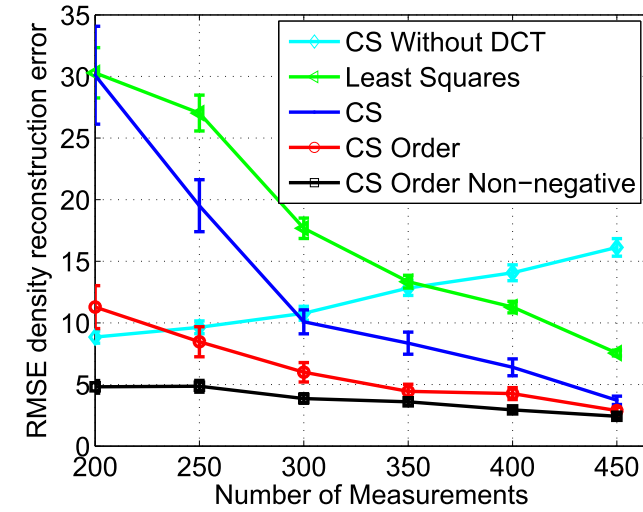


(b)

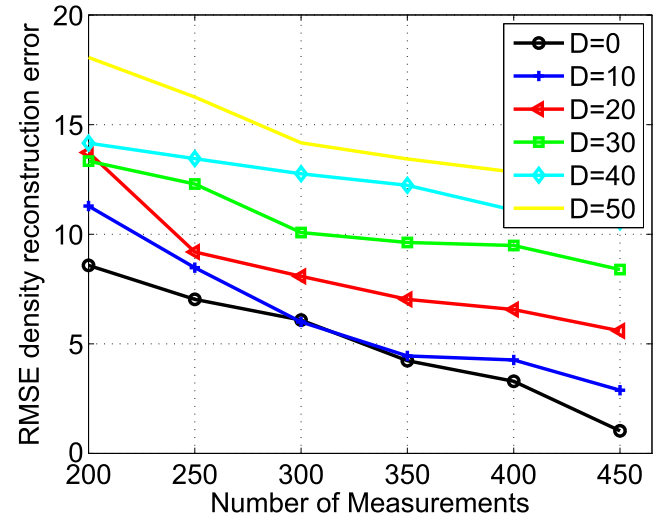


(c)

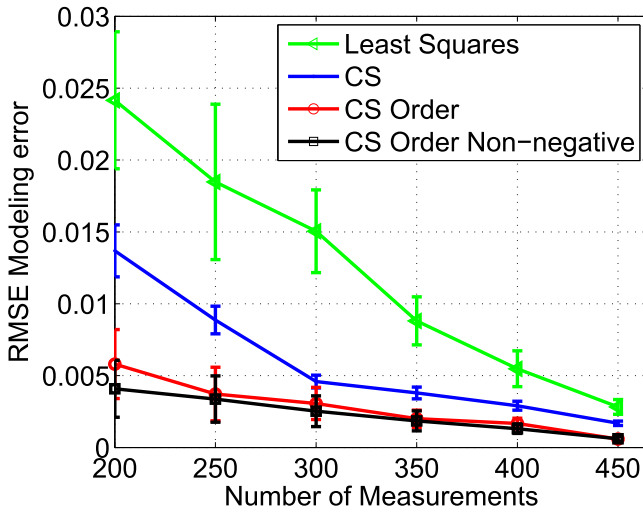
**Figure 3.** (a) Signal  $q$  showing the sparseness; (b) signal  $q_{\text{order}}$  is more approximately sparse than  $q$ ; (c) the reconstruction performance comparison based on ‘CS’ and ‘CS Order’.



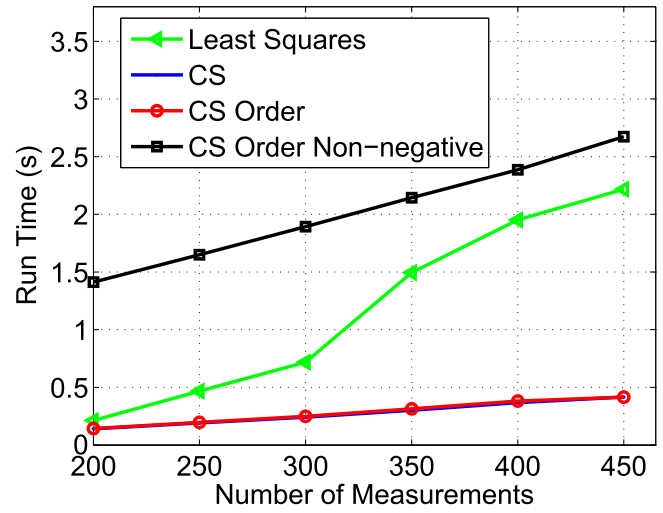
(a)



(a)



(b)



(b)

**Figure 4.** (a) Density  $w$  reconstruction error comparison; (b) the modeling error comparison.

Squares'. Among these CS-related approaches, 'CS' is the worst, and 'CS Order Non-negative' is consistently the best. On average, the RMSE errors of reconstructed density based on 'CS Order Non-negative', 'CS Order', and 'CS' are 28.1%, 34.5%, and 73.1% of the error using 'Least Squares', respectively. The 'CS Without DCT' cannot faithfully reconstruct the density, and the construction error is higher with more measurements, due to the fact that the density vector is not approximately sparse, and the measurement matrix does not follow the RIP condition, and thus this approach is not considered further in the rest of this paper. Figure 4(b) shows the normalized modeling error comparison. On average, the RMSE errors based on 'CS Order Non-negative', 'CS Order', and 'CS' are 18.3%, 22.6%, and 47.2% of the error using 'Least Squares', respectively.

Based on *Proposition 2*, the CS-related approaches have bounded reconstruction error under bounded measurement

**Figure 5.** (a) Density reconstruction error with varying measurement noise based on 'CS'; (b) the average identification run-time comparison.

noise. It is shown that when the magnitude of the bound for the measurement noise increases, the magnitude of the reconstruction error becomes larger. With the measurement noise following a uniform distribution on the interval  $[-\frac{D}{2}, \frac{D}{2}]$ , figure 5(a) shows the corresponding density reconstruction RMSE with varying amplitudes of measurement noise. Figure 5(b) shows the average run-time between the CS-related approaches and the least-squares algorithm. The computations are run in Matlab on a computer with Intel (R) Core(TM) i7-2600 3.40 GHz CPU and 4.00 GB memory. It is seen that when the number of measurements is increasing, 'CS' and 'CS Order' are much more efficient than 'Least Squares'. The ordering of the output consumes much less time than the generic path-following primal-dual method for solving the compressive sensing-based reconstruction algorithm. 'CS Order Non-negative' is slightly more time-



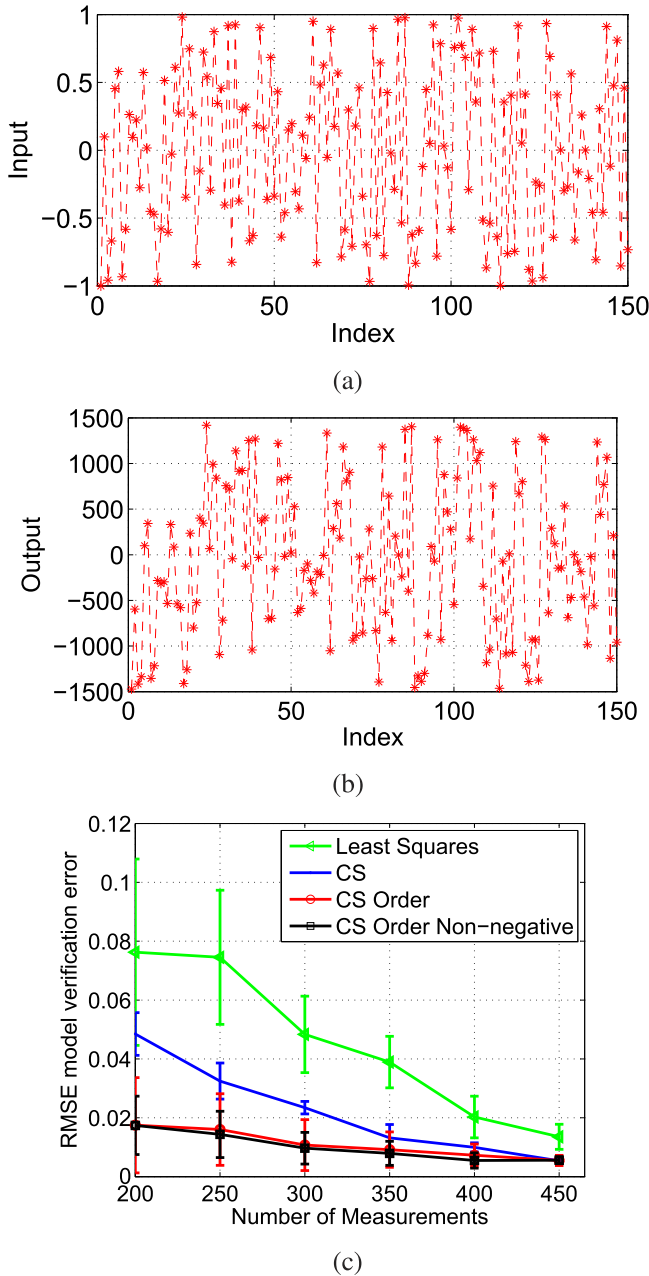


**Figure 6.** (a) A random input sequence for model validation; (b) corresponding output under the random input sequence in (a); (c) model estimation error comparison.

consuming than the ‘Least Squares’ approach, while it can ensure that the identified density function contains no negative elements. On average, the identification run-time of ‘Least Squares’, ‘CS’, ‘CS Order’, and ‘CS Order Non-negative’ are 1.18 s, 0.28 s, 0.29 s, and 1.99 s, respectively.

To further validate the proposed approach, a random input sequence shown in figure 6(a) is used, figure 6(b) shows the corresponding output corrupted with a noise that has the aforementioned distribution with  $D = 20$ . Figure 6(c) shows the normalized model estimation error comparison under the random input. On average, the RMSE errors of reconstructed density based on ‘CS Order Non-negative’, ‘CS Order’, and ‘CS’ are 22.3%, 24.4%, and 48.8% of the error using ‘Least

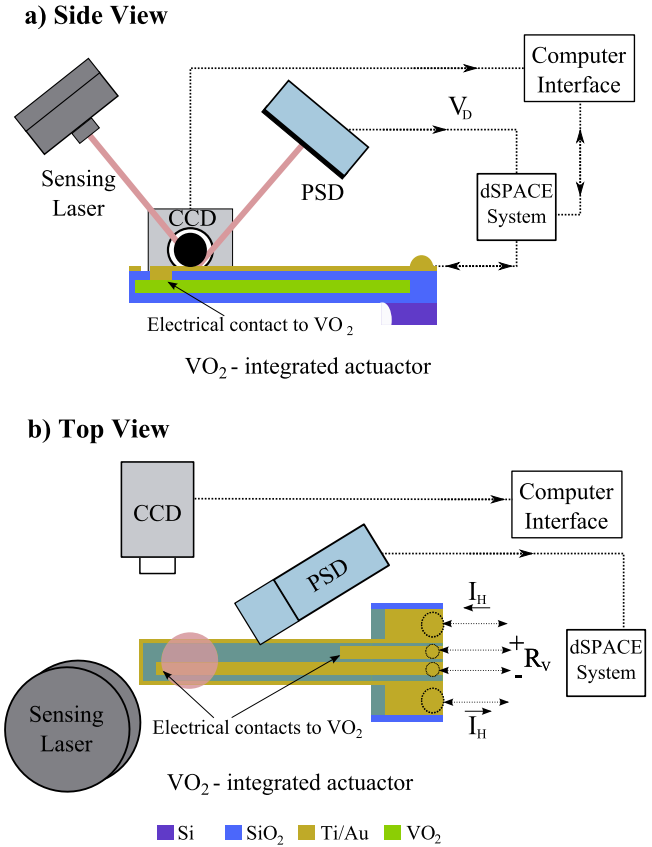


**Figure 7.** (a) Side view schematic for the measurements setup for deflection of a microactuator with an integrated heater; (b) Top view of the VO<sub>2</sub>-based integrated actuator devices.

Squares’, respectively. For example, when the number of measurements is 300, the average RMSE errors using ‘Least Squares’, ‘CS’, ‘CS Order’, and ‘CS Order Non-negative’ are 0.048, 0.024, 0.011, and 0.010, respectively.

## 5. Experimental results

VO<sub>2</sub> is an interesting class of smart materials with a myriad of microactuation, optical, and memory applications. It undergoes an insulator-to-metal transition at around 68 °C, during which resistance [20], induced mechanical stress [6], and optical transmittance demonstrate pronounced hysteresis. The proposed identification algorithm is verified in experiments for identifying and characterizing the hysteresis between the voltage input and the deflection output of a VO<sub>2</sub>-integrated microactuator.

### 5.1. Measurement setup

The experimental setup used is shown in figure 7(a). The microactuator used in this setup consisted of a silicon dioxide (SiO<sub>2</sub>) microcantilever with patterned VO<sub>2</sub> film inside the structure and a patterned metal layer (Au/Ti) on top. The VO<sub>2</sub> film was used as the active actuation element in the cantilever, while the metal layer was used to form the heating element and the traces for the VO<sub>2</sub> resistance contacts. The measurement system was based on a laser scattering technique, using an IR

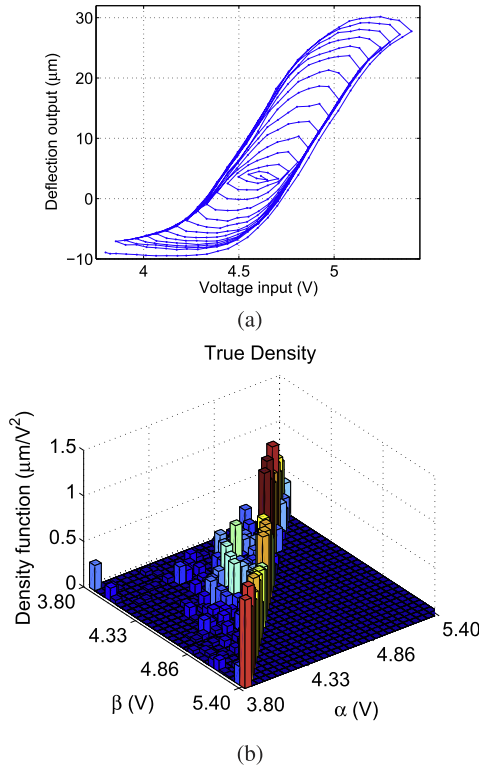


**Figure 8.** (a) Input-output data for identifying Preisach model ( $L = 30$ ); (b) true density function identified based on 467 measurements.

laser ( $\lambda = 985$  nm) and a position sensitive detector (PSD) to track the displacement of the microactuator. A charge couple device (CCD) camera was used for alignment and calibration purposes. A data acquisition system and field programmable gate array (DAQ/FPGA) with a computer interface was used to automate the control/monitor of electric signals. The power of the sensing laser (10 mW) was calibrated to be the minimum possible to be sensed by the PSD without heating the cantilever due to photon absorption. The voltage output (VD) of the PSD was linearly proportional to the position of the laser. Using images captured by the CCD camera, this voltage (VD) was mapped to the deflection of the cantilever. The chip was inside a side braze packaging (wire-bonded), which was connected to the DAQ/FPGA. The current  $I_H$  shown in figure 7(b) was used to control the temperature of the microactuator by Joule heating. The current was generated using two resistances in series: the heater resistance and an external resistance, whose only purpose was to limit the maximum current (12.78 mA) that can be applied to the system. An input voltage from the DAQ/FPGA and the computer interface was used to generate this current.

### 5.2. Identification and verification

A  $\text{VO}_2$ -integrated silicon microactuator is subject to two actuation effects when its temperature is varied [6]. The first is the phase transition-induced stress, which makes the beam bend towards the  $\text{VO}_2$  layer when the microactuator is heated. The deflection due to phase transition can be modeled by a Preisach model. The second effect is the differential thermal expansion-

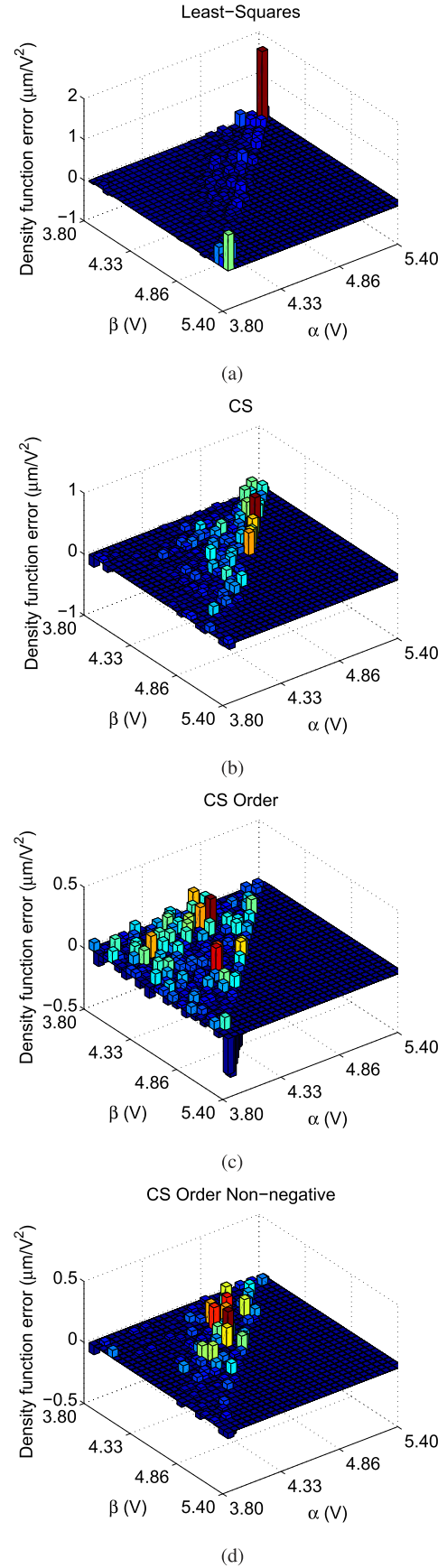


**Figure 9.** Density reconstruction error comparison based on (a) Least Squares; (b) CS; (c) CS Order; (d) CS Order Non-negative approaches.

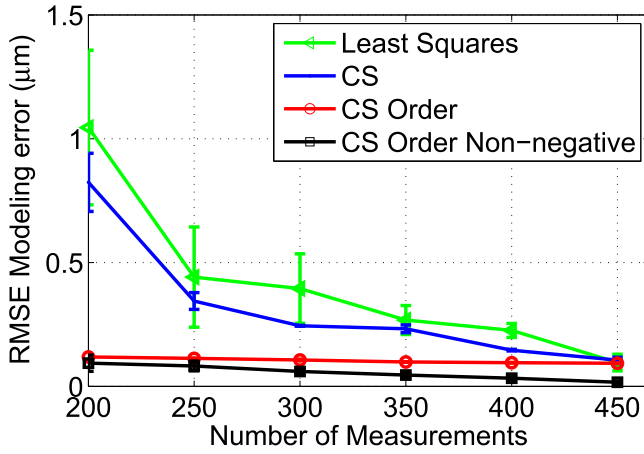


Figure 10. The average RMSE modeling error comparison.

induced stress, which makes the beam bend away from the  $\text{VO}_2$  layer under heating. The latter effect is modeled with a linear term. As a result, the hysteresis between the deflection and the temperature is non-monotonic, and can be modeled as

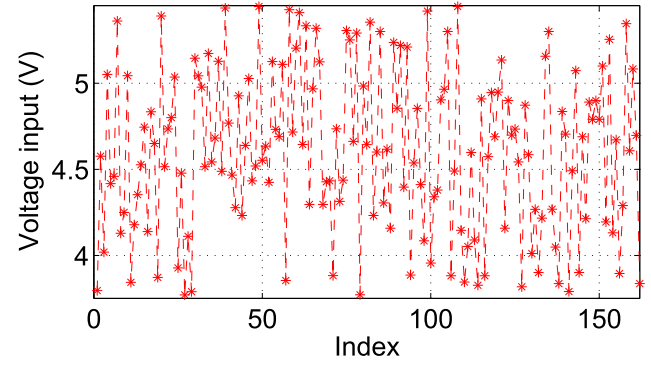
$$\tilde{u}(n) = \mu_0 + c_d v(n) + \sum_{i=1}^L \sum_{j=1}^{L+1-i} \mu_{ij} s_{ij}(n). \quad (22)$$

The model expressed in equation (20) can be expressed in the form of equation (4). Take discretization level  $L = 30$  as an example, where  $w$  contains  $N = L(L+1)/2 + 2 = 467$  elements, and can be written as  $w = (w_1 w_2 \cdots w_{L(L+1)/2} \mu_0 c_d)^T$ . Apply the following input sequence to the system: the first 466 elements are the same as a damped oscillation sequence shown in figure 2, the 467th element of the input can be any value other than 0 to ensure that the corresponding matrix  $S$  is invertible.  $S$  is a  $467 \times 467$  matrix, where  $S(n, k) = s_{ij}(n)$ ,  $S(n, L(L+1)/2 + 1) = 1$ , and  $S(n, L(L+1)/2 + 2) = v[n]$ . Figure 8(a) shows the non-monotonic hysteresis behavior between the voltage input and the deflection output. Figure 8(b) shows the corresponding density function (true density) identified based on the 467 measurements shown in figure 8(a).

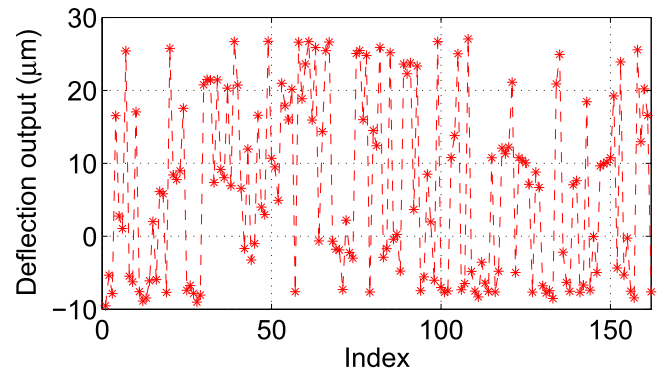
It can be proved that by applying the aforementioned input sequence, the rank of the corresponding  $S$  is 467. Instead of utilizing all of the 467 corresponding output deflection measurements, a subset of the output measurements were randomly chosen for identification. For each number of measurements used in the compressive sensing algorithms and least-squares scheme, the reconstruction algorithms are run 1000 times (thus with different sets of chosen input-output data), and the performance is averaged over all runs.

When the number of measurements used for identification is 300, figures 9(a)–(d) show typical density function reconstruction error comparisons. It is calculated that the RMSE error using ‘Least Squares’, ‘CS’, ‘CS Order’, and ‘CS Order Non-negative’ are  $0.122 \mu\text{m V}^{-2}$ ,  $0.116 \mu\text{m V}^{-2}$ ,  $0.096 \mu\text{m V}^{-2}$ , and  $0.059 \mu\text{m V}^{-2}$ , respectively.

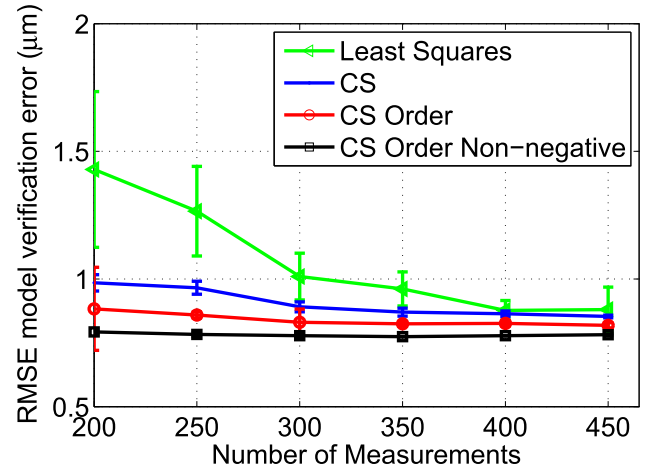
Figure 10 shows the normalized modeling error comparison. It is shown that ‘CS Order Non-negative’ consistently produces the smallest modeling error, followed by ‘CS Order’, ‘CS’, and ‘Least Squares’. On average, the



(a)



(b)



(c)

Figure 11. Density reconstruction error based on (a) a random input sequence for model validation; (b) output of the random input sequence in (a); (c) model estimation errors.

RMSE modeling errors based on ‘CS Order Non-negative’, ‘CS Order’, and ‘CS’ are 13.4%, 25.3%, and 76.8% of the error using ‘Least Squares’, respectively.

The effectiveness of the compressive sensing-based identification is further examined by comparing the model estimation performance under a random input shown in figure 11(a). The measured deflection output is shown in figure 11(b). Figure 11(c) shows the model estimation errors under the models identified with the compressive sensing

schemes and the least-squares scheme, respectively. On average over cases with different number of measurements, the RMSE of reconstructed density based on ‘CS Order Non-negative’, ‘CS Order’, and ‘CS’ are 72.9%, 78.4%, and 84.5% of the error using ‘Least Squares’, respectively. For example, when the number of measurements used for identification is 300, the average RMSE errors using ‘Least Squares’, ‘CS’, ‘CS Order’, and ‘CS Order Non-negative’ are  $1.010\text{ }\mu\text{m}$ ,  $0.891\text{ }\mu\text{m}$ ,  $0.831\text{ }\mu\text{m}$ , and  $0.778\text{ }\mu\text{m}$ , respectively. These findings are consistent with the simulation results.

## 6. Conclusion and future work

In this paper efficient and effective identification of the Preisach model was studied under the compressive sensing framework that required much fewer measurements. The proposed approach adopted the DCT transform of the output data to obtain a sparse vector. The proposed identification approach was shown to have better identification performance than the least-squares scheme through both simulation and experiments involving a  $\text{VO}_2$ -integrated microactuator. In future work, the transformation of the output data will be further studied to generate sparser vectors. The use of Moore-Penrose pseudoinverse will be studied for input sequences with a different number of entries with the number of the model parameters and the matrix  $S$  is not invertible. Compressive sensing for other types of hysteresis models, such as the Prandtl–Ishlinskii models, will also be studied.

## Acknowledgments

The  $\text{VO}_2$  microactuator used in this work was fabricated in part at the Lurie Nanofabrication Facility, a member of the National Nanotechnology Infrastructure Network, which is supported in part by the National Science Foundation.

## References

- [1] Jiles D and Atherton D 1986 Theory of ferromagnetic hysteresis *J. Magn. Magn. Mater.* **61** 48–60
- [2] Tan X and Baras J 2005 Adaptive identification and control of hysteresis in smart materials *IEEE Trans. Autom. Control* **50** 827–39
- [3] Tan X, Venkataraman R and Krishnaprasad P S 2001 Control of hysteresis: theory and experimental results *Smart Structures and Materials 2001: Modeling, Signal Processing, and Control in Smart Structures* pp 101–12
- [4] Li Z, Su C-Y and Chai T 2014 Compensation of hysteresis nonlinearity in magnetostrictive actuators with inverse multiplicative structure for Preisach model *IEEE Trans. Autom. Sci. Eng.* **11** 613–9
- [5] Tan X and Baras J S 2004 Modeling and control of hysteresis in magnetostrictive actuators *Automatica* **40** 1469–80
- [6] Zhang J, Merced E, Sepúlveda N and Tan X 2014 Modeling and inverse compensation of non-monotonic hysteresis in  $\text{VO}_2$ -coated microactuators *IEEE/ASME Trans. Mech.* **19** 579–88
- [7] Al Janaideh M, Rakheja S and Su C-Y 2009 A generalized Prandtl–Ishlinskii model for characterizing the hysteresis and saturation nonlinearities of smart actuators *Smart Mater. Struct.* **18** 045001
- [8] Sun Z, Song B, Xi N, Yang R, Hao L and Chen L 2015 Compensating asymmetric hysteresis for nanorobot motion control *Proc. IEEE Int. Conf. on Robotics and Automation (ICRA)* pp 3501–6
- [9] Vo-Minh T, Tjahjowidodo T, Ramon H and Brussel H V 2011 A new approach to modeling hysteresis in a pneumatic artificial muscle using the maxwell-slip model *IEEE/ASME Trans. Mech.* **16** 177–86
- [10] Liu Y, Shan J and Gabbert U 2015 Feedback/feedforward control of hysteresis-compensated piezoelectric actuators for high-speed scanning applications *Smart Mater. Struct.* **24** 015012
- [11] Xu Q and Wong P 2011 Hysteresis modeling and compensation of a piezostage using least squares support vector machines *Mechatronics* **21** 1239–51
- [12] Habineza D, Rakotondrabe M and Gorrec Y Le 2015 Bouc–Wen modeling and feedforward control of multivariable hysteresis in piezoelectric systems: application to a 3-dof piezotube scanner *IEEE Trans. Control Syst. Technol.* **23** 1797–806
- [13] Oh J and Bernstein D 2005 Semilinear Duhem model for rate-independent and rate-dependent hysteresis *IEEE Trans. Autom. Control* **50** 631–45
- [14] Wang X, Alici G and Tan X 2014 Modeling and inverse feedforward control for conducting polymer actuators with hysteresis *Smart Mater. Struct.* **23** 025015
- [15] Brokate M and Sprekels J 1996 *Hysteresis and Phase Transitions* (Berlin: Springer)
- [16] Visintin A 1994 *Differential Models of Hysteresis* (Berlin: Springer)
- [17] Ruderman M 2013 Direct recursive identification of the Preisach hysteresis density function *J. Magn. Magn. Mater.* **348** 22–6
- [18] Iyer R and Tan X 2009 Control of hysteretic systems through inverse compensation: inversion algorithms, adaptation, and embedded implementation *IEEE Control Syst. Mag.* **29** 83–99
- [19] Zhang J, Merced E, Sepúlveda N and Tan X 2013 Kullback–Leibler divergence-based optimal compression of Preisach operator in hysteresis modeling *Proc. American Control Conf. (ACC)* pp 89–94
- [20] Zhang J, Merced E, Sepúlveda N and Tan X 2015 Optimal compression of generalized Prandtl–Ishlinskii hysteresis models *Automatica* **57** 170–9
- [21] Candes E, Romberg J and Tao T 2006 Robust uncertainty principles: exact signal reconstruction from highly incomplete frequency information *IEEE Trans. Inform. Theor.* **52** 489–509
- [22] Rudelson M and Vershynin R 2008 On sparse reconstruction from Fourier and Gaussian measurements *Commun. Pur. Appl. Math.* **61** 1025–45
- [23] Candes E and Wakin M 2008 An introduction to compressive sampling *IEEE Signal Proc. Mag.* **25** 21–30
- [24] Candes E, Romberg J K and Tao T 2006 Stable signal recovery from incomplete and inaccurate measurements *Commun. Pur. Appl. Math.* **59** 1207–23
- [25] Zhao J, Song B, Xi N, Lai K W C, Chen H and Qu C 2012 Compressive feedback based non-vector space control *Proc. American Control Conf. (ACC)* pp 4090–5
- [26] Moreno-Alvarado R G and Martinez-Garcia M 2011 DCT-compressive sampling of frequency-sparse audio signals *Proc. World Congress on Engineering* pp 627–31
- [27] Deng C, Lin W, Lee B-S and Lau C 2010 Robust image compression based on compressive sensing *Proc. IEEE International Conf. on Multimedia and Expo (ICME)* pp 462–7

- [28] Maxwell B and Andersson S 2014 A compressed sensing measurement matrix for atomic force microscopy *Proc. American Control Conf. (ACC)* pp 1631–6
- [29] Duarte M, Davenport M, Takhar D, Laska J, Sun T, Kelly K and Baraniuk R 2008 Single-pixel imaging via compressive sampling *IEEE Signal Proc. Mag.* **25** 83–91
- [30] Chang Y H and Tomlin C 2012 Data-driven graph reconstruction using compressive sensing *Proc. Decision and Control Conf. (CDC)* pp 1035–40
- [31] OConnor S M, Lynch J P and Gilbert A C 2014 Compressed sensing embedded in an operational wireless sensor network to achieve energy efficiency in long-term monitoring applications *Smart Mater. Struct.* **23** 085014
- [32] Wright J, Yang A, Ganesh A, Sastry S and Ma Y 2009 Robust face recognition via sparse representation *IEEE Trans. Pattern Anal.* **31** 210–27
- [33] Toth R, Sanandaji B, Poolla K and Vincent T 2011 Compressive system identification in the linear time-invariant framework *Proc. Decision and Control and European Control Conf. (CDC–ECC)* pp 783–90
- [34] Zhang J, Merced E, Sepúlveda N and Tan X 2015 Compressive sensing-based Preisach hysteresis model identification *Proc. of American Control Conf. (ACC)* pp 2637–42
- [35] Ben-Israel A and Greville T 2006 *Generalized Inverses: Theory and Applications (CMS books in Mathematics)* (New York: Springer)